Vol 16 No 10, October 2007
1009-1963/2007/16(10)/2984-09

Chinese Physics

© 2007 Chin. Phys. Soc.
and IOP Publishing Ltd

Dressed multi-wave mixing in a V-type four-level atomic system*

Jiang Tong(姜 彤)[a], Zhang Yan-Peng(张彦鹏)[a)b)†], Nie Zhi-Qiang(聂志强)[a], Li Ling(李 岭)[a], Li Pei-Zhe(李沛哲)[a], Shen Lei-Jian(沈磊剑)[a], Fu Xin(傅 鑫)[a], Gan Chen-Li(甘琛利)[b], Zhao Rong-Kuo(赵荣阔)[a], Song Jian-Ping (宋建平)[a], and Lu Ke-Qing(卢克清)[c]

[a] *Key Laboratory for Physical Electronics and Devices of the Ministry of Education, Xi'an Jiaotong University, Xi'an* 710049, *China*
[b] *Department of Physics, University of Arkansas, Fayetteville, Arkansas* 72701, *USA*
[c] *State Key Laboratory of Transient Optics and Technology, Xi'an Institute of Optics and Precision Mechanics, Chinese Academy of Sciences, Xi'an* 710068, *China*

(Received 27 November 2006; revised manuscript received 16 April 2007)

The dressed four- and six-wave mixings in a V-type four-level system are considered. Under two different dressed conditions, two- and three-photon resonant Autler–Townes splittings, accompanied by enhancement and suppression of wave mixing signal, are obtained analytically. Meanwhile, an electromagnetic induced transparency of multi-wave mixing is presented, which shows multiple peaks and asymmetric effects caused by one-photon, two-photon and three-photon resonances, separately. The slow light propagation multiple region of multi-wave mixing signal is also obtained.

Keywords: Autler–Townes splitting, electromagnetic induced transparency, multi-wave mixing
PACC: 4250, 3280

1. Introduction

Four-wave mixing (FWM) is a third-order nonlinear optical process in which three input beams induce a nonlinear polarization in a medium, giving rise to the generation of a fourth coherent beam. The FWM signal is directly related to a third-order nonlinear susceptibility $\chi^{(3)}$, which exhibits resonant characteristics of the medium. Harris[1] has proposed a concept of electromagneticcally induced transparency (EIT) which renders a resonant transition transparent. The key idea of EIT is to use a strong-coupling field between the metastable and upper states to dress them equivalently as two states decaying to a common level or continuum, and to induce the transparency at the split-centre of Autler–Townes (AT) components. Owing to the reduced absorption, the EIT effect in an optically thick medium has possible applications in nonlinear optics, lasing without population inversion, dispersion enhancement, and quantum noise reduction.[2] In four-level atomic systems, more energy level configurations can be envisioned, and nonlinear optical processes can be optimized by suppressing linear absorption through EIT (destructive interference) and increasing the nonlinear optical coefficient through constructive interferences in three-photon processes.[3−6]

The physics of wave-mixing interactions has been a subject of intensive research in the past few decades. Various types of nonlinear spectroscopy based on wave mixing are capable of addressing dynamic information related to the structure of matter because the nonlinear susceptibility exhibits resonances at the natural frequencies of media. In this four-level system a new type of FWM and six-wave mixing (SWM) in a dressed atomic system has been studied, where two different systems on condition that the location of coupling field changes between two different energy levels, $|1\rangle$ and $|2\rangle$ or $|0\rangle$ and $|3\rangle$, are investigated, which both present a multiple-photon AT-splitting. This process provides a spectroscopic tool for measuring not only the resonant frequency and dephasing rate but also the transition dipole moment between two highly excited atomic states. Also higher-order wave-mixing effects have been observed in several ex-

*Project supported by the National Natural Science Foundation of China (Grant Nos 60308002 and 60678005), the Foundation for the Author of National Excellent Doctoral Dissertation of China (Grant No 200339), the Foundation for Key Program of Ministry of Education,China (Grant No 105156), the For Ying-Tong Education Foundation for Young Teachers in the Institutions of Higher Education of China (Grant No 101061) and the Specialized Research Fund for the Doctoral Program of Higher Education of China (Grant No 20050698017).
†Corresponding author. E-mail: ypzhang@mail.xjtu.edu.cn

periments. However, one of the difficulties encountered is that as the order of the nonlinearity increases, more complex beam geometries are usually required to satisfy the phase-matching conditions. Moreover, the nonlinear signal decreases by several orders of magnitude with the increase of the degree of nonlinearity of the interaction.[3−6] In this paper the multiple wave-mixing in this four-level system is studied, and the EIT phenomena show multiple peaks caused by multiple-photon resonance. Diagonal population is obtained, and the signal intensity simulation with multiple peaks is also carried out. The slow light phenomena are also studied in the last part where the multi-wave mixing signal propagates more slowly at several points.

2. Basic theory

We consider a V-type four-level system (see Fig.1(b) and Fig.1(d)), in which states between $|0\rangle$ and $|1\rangle$, $|1\rangle$ and $|2\rangle$, and $|0\rangle$ and $|3\rangle$ are dipole-allowed transitions with resonant frequencies Ω_1, Ω_2 and Ω_3 and dipole moments μ_1, μ_2 and μ_3, respectively.

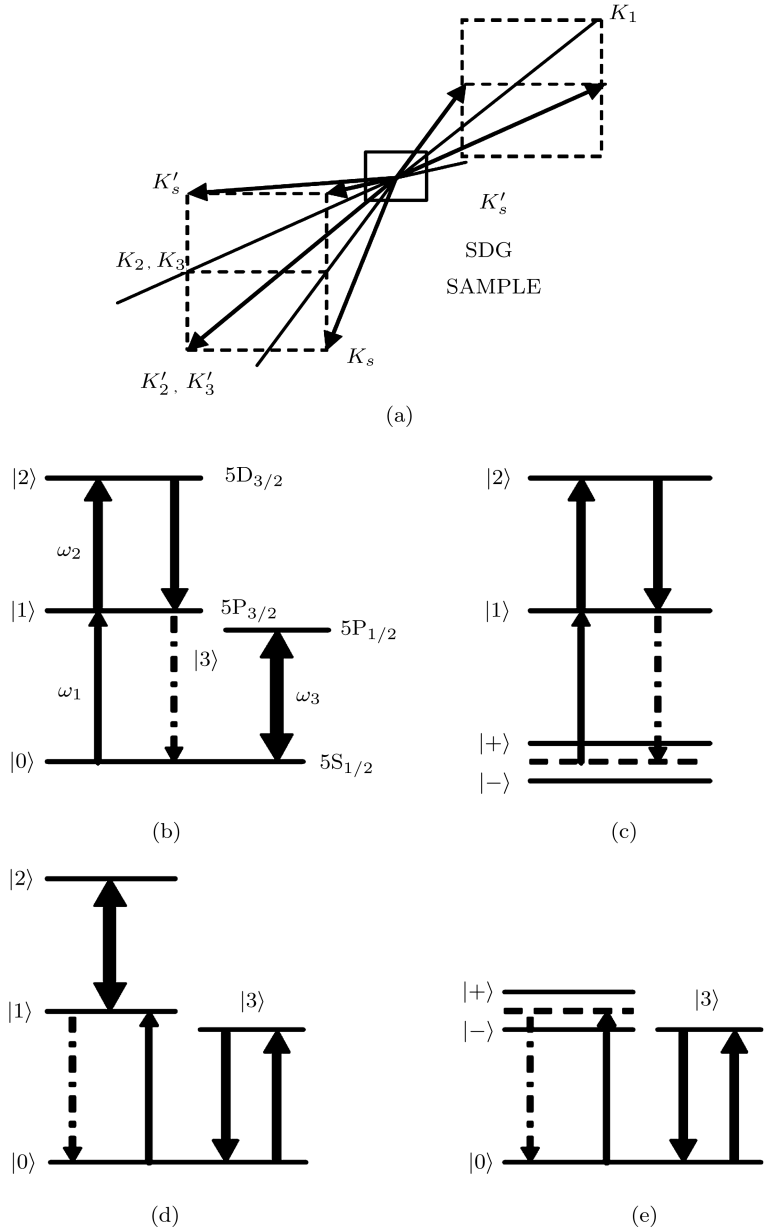


Fig.1. Three-dimensional beam geometry (a), four-level diagram with an ω_3 coupling field (b), four-level diagram with an ω_2 coupling field (d), and dressed NDFWM schemes (c) and (e) corresponding to (b) and (d), respectively.

From Fig.1(c), a two-photon resonance of non-degenerate four-wave mixing (NDFWM) in a $|0\rangle$-$|1\rangle$-$|2\rangle$ cascade three-level system is obtained by blocking the laser $\boldsymbol{k}_3'$, and the diffracted signals will be generated along the directions $\boldsymbol{k}_{2\mathrm{d}}$ as indicated in Table 1. From Fig.1(d), a V-type three-level system is achieved by locking the laser $\boldsymbol{k}_2'$, and the diffracted signals will be generated along the directions $\boldsymbol{k}_{3\mathrm{d}}$ as shown in Table 1. Consider the beam geometry indicated in Fig.1(a) where the laser fields can be represented by $E_i = \varepsilon_i \mathrm{e}^{\mathrm{i}\boldsymbol{k}_i\cdot\boldsymbol{r}-\mathrm{i}\omega_i t}$ and $E_i' = \varepsilon_i' \mathrm{e}^{\mathrm{i}\boldsymbol{k}_i'\cdot\boldsymbol{r}-\mathrm{i}\omega_i t}$ ($\omega_i \approx \Omega_i$). The fields that interact in the sample are combined by the six incident laser fields such that the diffracted signals with different diffraction orders can be produced. Assume that the crossing angles between the pump beams (E_2 and E_2', or E_3 and E_3') and the probe beams (E_1 and E_1') are adjusted so as to obtain a perfect wave vector phase matching for third-order diffractions ($\chi^{(3)}$ process). Thus, a signal beam at a frequency ω_1 will be emitted along the directions as shown in Table 1. At the same time, the crossing angles can also be chosen to be phase matched for fifth-order diffractions. Owing to $\chi^{(5)}$ involving the same probe beams, thus, diffracted signals will be generated along the same directions as those that are indicated in Table 1.

Table 1. FWM and SWM perturbation chains and corresponding phase matching conditions.

	Perturbation chain	Phase matching condition
FWM	$\rho_{00}^{(0)} \xrightarrow{\omega_1} \rho_{10}^{(1)} \xrightarrow{\omega_2} \rho_{20}^{(2)} \xrightarrow{-\omega_2} \rho_{10}^{(3)}$ (f1)	$\boldsymbol{k}_{2\mathrm{d}} = \boldsymbol{k}_1 + \boldsymbol{k}_2 - \boldsymbol{k}_2'$ $\boldsymbol{k}_{2\mathrm{d}}' = \boldsymbol{k}_1' + \boldsymbol{k}_2' - \boldsymbol{k}_2$
	$\rho_{00}^{(0)} \xrightarrow{\omega_3} \rho_{30}^{(1)} \xrightarrow{-\omega_3} \rho_{00}^{(2)} \xrightarrow{\omega_1} \rho_{10}^{(3)}$ (f2)	$\boldsymbol{k}_{3\mathrm{d}} = \boldsymbol{k}_3 - \boldsymbol{k}_3' + \boldsymbol{k}_1$
	$\rho_{00}^{(0)} \xrightarrow{-\omega_3} \rho_{03}^{(1)} \xrightarrow{\omega_3} \rho_{00}^{(2)} \xrightarrow{\omega_1} \rho_{10}^{(3)}$ (f3)	$\boldsymbol{k}_{3\mathrm{d}}' = \boldsymbol{k}_3' - \boldsymbol{k}_3 + \boldsymbol{k}_1'$
	$\rho_{00}^{(0)} \xrightarrow{\omega_1} \rho_{10}^{(1)} \xrightarrow{-\omega_3} \rho_{13}^{(2)} \xrightarrow{\omega_3} \rho_{10}^{(3)}$ (f4)	
	$\rho_{00}^{(0)} \xrightarrow{-\omega_3} \rho_{03}^{(1)} \xrightarrow{\omega_1} \rho_{13}^{(2)} \xrightarrow{\omega_3} \rho_{10}^{(3)}$ (f5)	
SWM	$\rho_{00}^{(0)} \xrightarrow{\omega_1} \rho_{10}^{(1)} \xrightarrow{\omega_2} \rho_{20}^{(2)} \xrightarrow{-\omega_3} \rho_{23}^{(3)} \xrightarrow{\omega_3} \rho_{20}^{(4)} \xrightarrow{-\omega_2} \rho_{10}^{(4)}$ (s1)	$\boldsymbol{k}_{2\mathrm{d}} = \boldsymbol{k}_1 + \boldsymbol{k}_3 - \boldsymbol{k}_3 + \boldsymbol{k}_2 - \boldsymbol{k}_2'$
	$\rho_{00}^{(0)} \xrightarrow{\omega_1} \rho_{10}^{(1)} \xrightarrow{\omega_3} \rho_{13}^{(2)} \xrightarrow{-\omega_3} \rho_{10}^{(3)} \xrightarrow{\omega_2} \rho_{20}^{(4)} \xrightarrow{-\omega_2} \rho_{10}^{(5)}$ (s2)	(or $\boldsymbol{k}_1 + \boldsymbol{k}_3' - \boldsymbol{k}_3' + \boldsymbol{k}_2 - \boldsymbol{k}_2'$)
	$\rho_{00}^{(0)} \xrightarrow{\omega_1} \rho_{10}^{(1)} \xrightarrow{\omega_2} \rho_{20}^{(2)} \xrightarrow{-\omega_2} \rho_{10}^{(3)} \xrightarrow{-\omega_3} \rho_{13}^{(4)} \xrightarrow{\omega_3} \rho_{10}^{(5)}$ (s3)	$\boldsymbol{k}_{2\mathrm{d}}' = \boldsymbol{k}_1' + \boldsymbol{k}_3 - \boldsymbol{k}_3 + \boldsymbol{k}_2' - \boldsymbol{k}_2$
	$\rho_{00}^{(0)} \xrightarrow{\omega_3} \rho_{30}^{(1)} \xrightarrow{-\omega_3} \rho_{00}^{(2)} \xrightarrow{\omega_1} \rho_{10}^{(3)} \xrightarrow{\omega_2} \rho_{20}^{(4)} \xrightarrow{-\omega_2} \rho_{10}^{(5)}$ (s4)	(or $\boldsymbol{k}_1 + \boldsymbol{k}_3' - \boldsymbol{k}_3' + \boldsymbol{k}_2' - \boldsymbol{k}_2$)
	$\rho_{00}^{(0)} \xrightarrow{-\omega_3} \rho_{03}^{(1)} \xrightarrow{\omega_3} \rho_{00}^{(2)} \xrightarrow{\omega_1} \rho_{10}^{(3)} \xrightarrow{\omega_2} \rho_{20}^{(4)} \xrightarrow{-\omega_2} \rho_{10}^{(5)}$ (s5)	$\boldsymbol{k}_{3\mathrm{d}} = \boldsymbol{k}_1 + \boldsymbol{k}_2 - \boldsymbol{k}_2 + \boldsymbol{k}_3 - \boldsymbol{k}_3'$
	$\rho_{00}^{(0)} \xrightarrow{\omega_1} \rho_{10}^{(1)} \xrightarrow{-\omega_3} \rho_{13}^{(2)} \xrightarrow{\omega_2} \rho_{23}^{(3)} \xrightarrow{-\omega_2} \rho_{13}^{(4)} \xrightarrow{\omega_3} \rho_{10}^{(5)}$ (s6)	(or $\boldsymbol{k}_1 + \boldsymbol{k}_2' - \boldsymbol{k}_2' + \boldsymbol{k}_3 - \boldsymbol{k}_3'$)
	$\rho_{00}^{(0)} \xrightarrow{-\omega_3} \rho_{03}^{(1)} \xrightarrow{\omega_1} \rho_{13}^{(2)} \xrightarrow{\omega_2} \rho_{23}^{(3)} \xrightarrow{-\omega_2} \rho_{13}^{(4)} \xrightarrow{\omega_3} \rho_{10}^{(5)}$ (s7)	$\boldsymbol{k}_{3\mathrm{d}}' = \boldsymbol{k}_1' + \boldsymbol{k}_2 - \boldsymbol{k}_2 + \boldsymbol{k}_3' - \boldsymbol{k}_3$
	$\rho_{00}^{(0)} \xrightarrow{-\omega_3} \rho_{03}^{(1)} \xrightarrow{\omega_1} \rho_{13}^{(2)} \xrightarrow{\omega_3} \rho_{10}^{(3)} \xrightarrow{\omega_2} \rho_{20}^{(4)} \xrightarrow{-\omega_2} \rho_{10}^{(5)}$ (s8)	(or $\boldsymbol{k}_1' + \boldsymbol{k}_2' - \boldsymbol{k}_2' + \boldsymbol{k}_3' - \boldsymbol{k}_3$)
	$\rho_{00}^{(0)} \xrightarrow{\omega_1} \rho_{10}^{(1)} \xrightarrow{\omega_2} \rho_{20}^{(2)} \xrightarrow{-\omega_3} \rho_{23}^{(3)} \xrightarrow{-\omega_2} \rho_{13}^{(4)} \xrightarrow{-\omega_3} \rho_{10}^{(5)}$ (s9)	$\boldsymbol{k}_{2\mathrm{d}3\mathrm{d}} = \boldsymbol{k}_1 + \boldsymbol{k}_2 - \boldsymbol{k}_2' + \boldsymbol{k}_3 - \boldsymbol{k}_3'$
	$\rho_{00}^{(0)} \xrightarrow{\omega_1} \rho_{10}^{(1)} \xrightarrow{-\omega_3} \rho_{13}^{(2)} \xrightarrow{\omega_2} \rho_{23}^{(3)} \xrightarrow{\omega_3} \rho_{20}^{(4)} \xrightarrow{-\omega_2} \rho_{10}^{(5)}$ (s10)	$\boldsymbol{k}_{2\mathrm{d}3\mathrm{d}}' = \boldsymbol{k}_1' + \boldsymbol{k}_2' - \boldsymbol{k}_2 + \boldsymbol{k}_3' - \boldsymbol{k}_3$
	$\rho_{00}^{(0)} \xrightarrow{-\omega_3} \rho_{03}^{(1)} \xrightarrow{\omega_1} \rho_{13}^{(2)} \xrightarrow{\omega_2} \rho_{23}^{(3)} \xrightarrow{\omega_3} \rho_{20}^{(4)} \xrightarrow{-\omega_2} \rho_{10}^{(5)}$ (s11)	

Table 2. Third- and fifth-order response functions of the perturbation chains (f1)–(f5) and (s1)–(s8) using double-sided Feynman diagrams (DSFD). Each diagram represents a distinct Liouville space pathway.

FWM perturbation chain	Dressed FWM (FWM$^{\pm}$) signal	Corresponding SWM chain
(f1)	$\rho_{\pm0}^{(0)} \xrightarrow{\omega_1} \rho_{10}^{(1)} \xrightarrow{\omega_2} \rho_{20}^{(2)} \xrightarrow{-\omega_2} \rho_{10}^{(3)}$	(s4)
	$\rho_{0\pm}^{(0)} \xrightarrow{\omega_1} \rho_{10}^{(1)} \xrightarrow{\omega_2} \rho_{20}^{(2)} \xrightarrow{-\omega_2} \rho_{10}^{(3)}$	(s5)
	$\rho_{00}^{(0)} \xrightarrow{\omega_1} \rho_{1\pm}^{(1)} \xrightarrow{\omega_2} \rho_{20}^{(2)} \xrightarrow{-\omega_2} \rho_{10}^{(3)}$	(s2)
	$\rho_{00}^{(0)} \xrightarrow{\omega_1} \rho_{10}^{(1)} \xrightarrow{\omega_2} \rho_{2\pm}^{(2)} \xrightarrow{-\omega_2} \rho_{10}^{(3)}$	(s1)
	$\rho_{00}^{(0)} \xrightarrow{\omega_1} \rho_{10}^{(1)} \xrightarrow{\omega_2} \rho_{20}^{(2)} \xrightarrow{-\omega_2} \rho_{1\pm}^{(3)}$	(s3)
(f2)	$\rho_{00}^{(0)} \xrightarrow{\omega_3} \rho_{30}^{(1)} \xrightarrow{-\omega_3} \rho_{00}^{(2)} \xrightarrow{\omega_1} \rho_{\pm0}^{(3)}$	(s4)
(f3)	$\rho_{00}^{(0)} \xrightarrow{-\omega_3} \rho_{03}^{(1)} \xrightarrow{\omega_3} \rho_{00}^{(2)} \xrightarrow{\omega_1} \rho_{\pm0}^{(3)}$	(s5)
(f4)	$\rho_{00}^{(0)} \xrightarrow{\omega_1} \rho_{\pm0}^{(1)} \xrightarrow{-\omega_3} \rho_{13}^{(2)} \xrightarrow{\omega_3} \rho_{10}^{(3)}$	(s3)
	$\rho_{00}^{(0)} \xrightarrow{\omega_1} \rho_{10}^{(1)} \xrightarrow{-\omega_3} \rho_{\pm3}^{(2)} \xrightarrow{\omega_3} \rho_{10}^{(3)}$	(s6)
	$\rho_{00}^{(0)} \xrightarrow{\omega_1} \rho_{10}^{(1)} \xrightarrow{-\omega_3} \rho_{13}^{(2)} \xrightarrow{\omega_3} \rho_{\pm0}^{(3)}$	(s2)
(f5)	$\rho_{00}^{(0)} \xrightarrow{-\omega_3} \rho_{03}^{(1)} \xrightarrow{\omega_1} \rho_{\pm3}^{(2)} \xrightarrow{\omega_3} \rho_{10}^{(3)}$	(s7)
	$\rho_{00}^{(0)} \xrightarrow{-\omega_3} \rho_{03}^{(1)} \xrightarrow{\omega_1} \rho_{13}^{(2)} \xrightarrow{\omega_3} \rho_{\pm0}^{(3)}$	(s8)

Therefore, the signal beam at a frequency ω_1 with a wave vector $\boldsymbol{k}_{2\mathrm{d}}$ or $\boldsymbol{k}_{3\mathrm{d}}$ is generated by nonlinear polarization $\rho_{10}(\omega_1) = \rho_{10}^{(3)}(\omega_1) + \rho_{10}^{(5)}(\omega_1)$ (FWM$^{\pm}$ + SWM). Only $\boldsymbol{k}_{2\mathrm{d}}$ and $\boldsymbol{k}_{3\mathrm{d}}$ directions (E_{f} and E_{s} in Fig.1(a)) are considered for our experimental case. There are two nonlinear windows of SWM and FWM signals through EIT. Multiple-photon interference leads to an interplay between these SWM and FWM coherent processes. From the viewpoint of physics, the suppression and enhancement of the dressed FWM (FWM$^{\pm}$) signals in the dressed-state picture (Fig.1(c) and (e)) are due to multiple-photon interference between the two FWM channels shown in Table 2.

The multiple-photon AT splitting, EIT effect and slow light phenomena of a four-level system are investigated and presented in the following parts.

3. Two- and three-photon resonant AT splittings

Two-photon resonant NDFWM is considered by blocking the laser $\boldsymbol{k}_3'$ in a $|0\rangle$-$|1\rangle$-$|2\rangle$ cascade three-level system and by blocking the laser $\boldsymbol{k}_2'$ in a V-type system. $\Delta_1 = \Omega_1 - \omega_1$, $\Delta_2 = \Omega_2 - \omega_2$ and $\Delta_3 = \Omega_3 - \omega_3$ represent field detunings. The nonlinear polarization corresponding to the two-photon resonant NDFWM signal is proportional to the off-diagonal density matrix element ρ_{10}, which can be obtained from density matrix equations with decaying terms Γ ($\hat{H}$ is the effective Hamiltonian term)

$$\frac{\partial\hat{\rho}(t)}{\partial t} = \frac{1}{\mathrm{i}\hbar}[\hat{H}_0 + \hat{H}_1(t), \hat{\rho}(t)] - \Gamma\hat{\rho}, \tag{1}$$

where $H_1 = -E\boldsymbol{\mu}$ and $\boldsymbol{\mu}$ is the transition dipole moment. The Rabi frequency are defined as $G_1 = \dfrac{\varepsilon_1\mu_1}{\hbar}$, $G_2 = \dfrac{\varepsilon_2\mu_2}{\hbar}$, $G_2' = \dfrac{\varepsilon_2'\mu_2}{\hbar}$, $G_3 = \dfrac{\varepsilon_3\mu_3}{\hbar}$ and $G_3' = \dfrac{\varepsilon_3'\mu_3}{\hbar}$. The actual electrical fields are $\boldsymbol{E}_1 = \varepsilon_1\mathrm{e}^{\mathrm{i}k_1\bullet\boldsymbol{r}}$ and $E_2 = \varepsilon_2\mathrm{e}^{\mathrm{i}k_2\bullet\boldsymbol{r}} + \varepsilon_2'\mathrm{e}^{\mathrm{i}k_2'\bullet r}$. The transverse relaxation rate is $\Gamma_{ij} = \dfrac{1}{2}(\gamma_{in} + \gamma_{jm})$, where γ_{in} and γ_{jm} correspond to spontaneous emissions. Assume that all of the populations are initially in the ground state $|0\rangle$, i.e. $\rho_{00}^{(0)} \approx 1$, then five FWM chains (f1), (f2), (f3), (f4) and (f5) will be applicable. From Eq.(1), the following density matrix dynamical equations are deduced. For chain (f1) we have

$$\frac{\partial\rho_{10}^{(1)}}{\partial t} = -\mathrm{i}D_1\rho_{10}^{(1)} + \mathrm{i}G_1\mathrm{e}^{\mathrm{i}k_1\cdot r}\rho_{00}^{(0)}, \tag{2}$$

$$\frac{\partial\rho_{20}^{(2)}}{\partial t} = -\mathrm{i}D_2\rho_{20}^{(2)} + \mathrm{i}G_2\mathrm{e}^{\mathrm{i}\boldsymbol{k}_2\cdot\boldsymbol{r}}\rho_{10}^{(1)}, \tag{3}$$

$$\frac{\partial\rho_{10}^{(3)}}{\partial t} = -\mathrm{i}D_1\rho_{10}^{(3)} + \mathrm{i}(G_2')^*\mathrm{e}^{-\mathrm{i}\boldsymbol{k}_2'\cdot\boldsymbol{r}}\rho_{20}^{(2)}. \tag{4}$$

Define $D_1 = \mathrm{i}\Delta_1 + \Gamma_{10}$, $D_2 = \mathrm{i}(\Delta_1 + \Delta_2) + \Gamma_{20}$, $D_3 = \mathrm{i}(\Delta_1 + \Delta_2 - \Delta_3) + \Gamma_{32}$, $D_4 = \mathrm{i}(\Delta_1 - \Delta_3) + \Gamma_{13}$, $D_5 = \mathrm{i}\Delta_3 + \Gamma_{30}$, $D_6 = -\mathrm{i}\Delta_3 + \Gamma_{03}$, $D_7 = \mathrm{i}\Delta_2 + \Gamma_{21}$, $D_8 = \mathrm{i}\Delta_2 + \Gamma_{20}$, $D_9 = \mathrm{i}(-\Delta_1 + \Delta_3) + \Gamma_{31}$, and $D_{10} = -\mathrm{i}\Delta_3 + \Gamma_{03}$, where $\Gamma_{10} = \gamma_{10}/2$, $\Gamma_{20} = (\gamma_{21} + \gamma_{23})/2$, $\Gamma_{30} = \gamma_{30}/2$, $\Gamma_{21} = (\gamma_{21} + \gamma_{10} + \gamma_{23})/2$, $\Gamma_{31} = (\gamma_{30} + \gamma_{10})/2$, and $\Gamma_{32} = (\gamma_{30} + \gamma_{21} + \gamma_{23})/2$. In a steady state, Eqs.(2), (3) and (4) are solved and the solution is

$$\rho_{\mathrm{FWM}}^{(\mathrm{f1})} = \frac{-\mathrm{i}U_1}{D_1^2D_2}. \tag{5}$$

In a similar way, the results of other four chains are deduced as follows: $\rho_{\mathrm{FWM}}^{(\mathrm{f2})} = \dfrac{-\mathrm{i}U_2}{\Gamma_{00}D_5D_1}$, $\rho_{\mathrm{FWM}}^{(\mathrm{f3})} = \dfrac{-\mathrm{i}U_2}{\Gamma_{00}D_1D_{10}}$, $\rho_{\mathrm{FWM}}^{(\mathrm{f4})} = \dfrac{-\mathrm{i}U_2}{D_1^2D_4}$ and $\rho_{\mathrm{FWM}}^{(\mathrm{f5})} = \dfrac{-\mathrm{i}U_2}{D_1D_6D_4}$.

3.1. With a coupling field of frequency ω_3

A V-type four-level system (Fig.1(b)) is discussed in this part. By blocking k_3', a cascade three-level system is generated. A coupling field of frequency ω_3 ($\approx \Omega_3$) is applied between $|0\rangle$ and $|3\rangle$; ω_1 and ω_2 are frequencies of probe and pump fields, respectively. How this coupling field affects the signal beam is investigated below. Five perturbation chains i.e. (s1), (s2), (s3), (s4) and (s5), are used. Using the partially rotating wave approximation, the dressed FWM expressions for these five chains are deduced for a steady state. ε_1, ε_2' and ε_2 are assumed to be weak, whereas the coupling field ε_3 can be an arbitrary value. In the case of strong coupling field, using the partially rotating wave approximation, the total result of dressed FWM is deduced as

$$\begin{aligned}\rho_{\mathrm{DressedF1}}^{(3)} &= \rho_{\mathrm{DressedF}}^{(\mathrm{s1})} + \rho_{\mathrm{DressedF}}^{(\mathrm{s2})} + \rho_{\mathrm{DressedF}}^{(\mathrm{s3})} + \rho_{\mathrm{DressedF}}^{(\mathrm{s4})} + \rho_{\mathrm{DressedF}}^{(\mathrm{s5})} \\ &= \frac{-\mathrm{i}U_1D_3}{D_1^2(D_2D_3 + |G_3|^2)} + \frac{-\mathrm{i}U_1D_4}{D_1D_2(D_1D_4 + |G_3|^2)} + \frac{-\mathrm{i}U_1D_4}{D_1D_2(D_1D_4 + |G_3|^2)} + \rho_{\mathrm{DressedF}}^{(\mathrm{s4})} + \rho_{\mathrm{DressedF}}^{(\mathrm{s5})},\end{aligned}$$

where the last two parts $\rho^{(s4)}_{\mathrm{DressedF}}$ and $\rho^{(s5)}_{\mathrm{DressedF}}$ are special terms because the coupling field is applied between $|0\rangle$ and $|3\rangle$. The ground state $|0\rangle$ leads to such a complex circumstance that the results of two chains (s4) and (s5) may not have the AT-splitting phenomena similar to those that are obtained in other chains. Hence, only the results of other three chains are discussed here. Therefore, we can have

$$\rho^{(3)}_{\mathrm{DressedF1}} = \rho^{(s1)}_{\mathrm{DressedF}} + \rho^{(s2)}_{\mathrm{DressedF}} + \rho^{(s3)}_{\mathrm{DressedF}}. \quad (6)$$

From expression (6) the AT spectrum is first investigated. Figure 2(a) below shows that as G_3 increases, the spectrum splits into two separate peaks, and then they shift apart. The two peaks are located symmetrically with respect to $\Delta_1 = 0$ when the coupling field is exactly in resonance, and two peaks turn into asymmetrical ones depending on Δ_3 and $\Delta_3 - \Delta_2$, which are called two- and three-photon AT splittings. Figure 2(b) shows the Δ_3-dependence of the signal intensity. It can be seen that the signal intensity is suppressed when the frequency of the coupling field is scanned across the resonance.

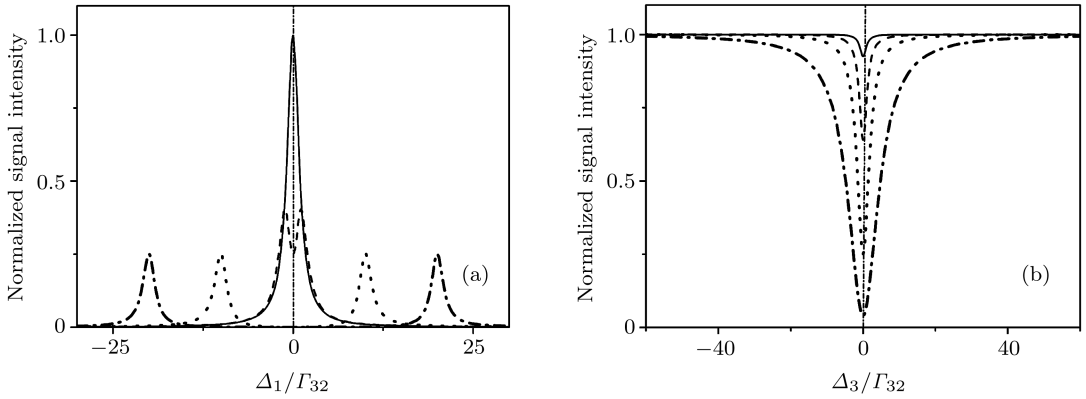


Fig.2. NDFWM signal intensity versus Δ_1/Γ_{32} (a), where $G_3 = 0$ (solid), Γ_{32} (dash), $10\Gamma_{32}$ (dot), and $20\Gamma_{32}$ (dash dot) and $\Delta_3 = 0$, and Δ_3-dependence of the NDFWM signal intensity at exact two-photon resonance (b), where $\Delta_1 = 0$, $G_3 = 0.2\Gamma_{32}$ (solid), $0.5\Gamma_{32}$ (dash), Γ_{32} (dot) and $2\Gamma_{32}$ (dash dot). The maximum of the NDFWM signal intensity with $G_3 = 0$ is normalized to 1. Parameters used here are: $\Gamma_{20} = \Gamma_{32}$, $\Gamma_{10} = \Gamma_{32}$, $\Delta_2 = 0$ and $\Gamma_{13} = \Gamma_{32}$.

3.2. With a coupling field of frequency ω_2

A V-type four-level system (Fig.1(d)) is also simulated. A V-type three-level system can be obtained by blocking laser k_2' and adding a coupling field of frequency $\omega_2(\approx \Omega_2)$ between $|1\rangle$ and $|2\rangle$. Similarly, a dressed FWM expression can be obtained for a V-type four-level system in Fig1.(d). The total results of this system can be written as

$$\begin{aligned}\rho^{(3)}_{\mathrm{DressedF2}} &= \rho^{(s2)}_{\mathrm{DressedF}} + \rho^{(s3)}_{\mathrm{DressedF}} + \rho^{(s4)}_{\mathrm{DressedF}} + \rho^{(s5)}_{\mathrm{DressedF}} + \rho^{(s6)}_{\mathrm{DressedF}} + \rho^{(s7)}_{\mathrm{DressedF}} + \rho^{(s8)}_{\mathrm{DressedF}} \\ &= \frac{-\mathrm{i}U_2D_2}{D_1D_4(D_2D_1+|G_2|^2)} + \frac{-\mathrm{i}U_2D_2}{D_1D_4(D_2D_1+|G_2|^2)} + \frac{-\mathrm{i}U_2D_2}{\Gamma_{00}D_5(D_1D_2+|G_2|^2)} + \frac{-\mathrm{i}U_2D_2}{\Gamma_{00}D_6(D_1D_2+|G_2|^2)} \\ &\quad + \frac{-\mathrm{i}U_2D_3}{D_1^2(D_3D_4+|G_2|^2)} + \frac{-\mathrm{i}U_2D_3}{D_1D_6(D_3D_4+|G_2|^2)} + \frac{-\mathrm{i}U_2D_2}{D_6D_4(D_1D_2+|G_2|^2)}, \end{aligned} \quad (7)$$

where we can find that chains (s4) and (s5) play an important role in the total expression, so only the results of these two perturbation chains are considered. Thus expression (6) becomes

$$\rho^{(3)}_{\mathrm{DressedF2}} = \rho^{(s4)}_{\mathrm{DressedF}} + \rho^{(s5)}_{\mathrm{DressedF}} = \frac{-\mathrm{i}U_2D_2}{\Gamma_{00}D_5(D_1D_2+|G_2|^2)} + \frac{-\mathrm{i}U_2D_2}{\Gamma_{00}D_6(D_1D_2+|G_2|^2)}. \quad (8)$$

From expression (8), with G_2 coupling field varying, the AT splitting and the intensity suppression are obtained (see Fig.3).

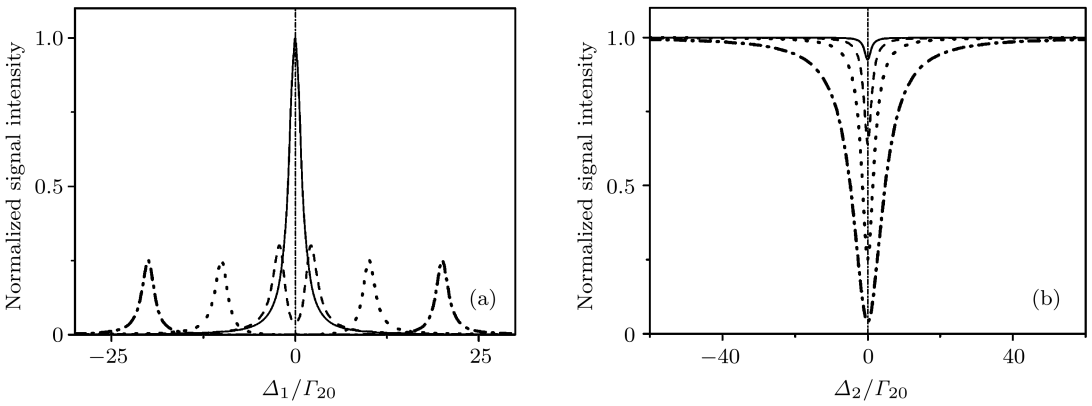


Fig.3. NDFWM signal intensity versus Δ_1/Γ_{20} (a), where $G_2 = 0$ (solid), Γ_{20} (dash), $10\Gamma_{20}$ (dot) and $20\Gamma_{20}$ (dash dot) and $\Delta_2 = 0$, and Δ_2-dependence of the NDFWM signal intensity at exact two-photon resonance (b), where $\Delta_1 = 0$, $G_2 = 0.2\Gamma_{20}$ (solid), $0.5\Gamma_{20}$ (dash), Γ_{20} (dot) and $2\Gamma_{20}$ (dash dot). The maximum of the NDFWM signal intensity with $G_2 = 0$ is normalized to 1. Parameters used here are $\Delta_3 = 0$, $\Gamma_{30} = \Gamma_{20}$, $\Gamma_{03} = \Gamma_{30}$ and $\Gamma_{10} = \Gamma_{20}$.

We can find from Fig.3(a), similar to Fig.2(a), that in this system when the coupling field is located at $|1\rangle$ and $|2\rangle$, there still exist two- and three-photon AT splittings. Figure 3(b) shows the suppression of Δ_2-dependence of the signal intensity, of which the features resemble those in Fig.2(b). The above investigation shows that the two different cases, with different beams k_2' and k_3' blocked, both exhibit an obvious AT-splitting in a dressed FWM system, moreover, the existence of a coupling field does not affect the phase matching condition.

3.3. Weak coupling field limit related to six-wave mixing (SWM)

In this part, the six-wave mixing will be deduced, which is described by perturbation chains (s1)–(s8). For chain (s1), after using the rotate wave approximation in $\dfrac{\partial\rho_{20}^{(4)}}{\partial t} = -D_2\rho_{20}^{(4)} - \mathrm{i}G_3\mathrm{e}^{\mathrm{i}\boldsymbol{k}_3\cdot\boldsymbol{r}}\rho_{23}^{(3)}$, $\rho_{20}^{(4)} = \dfrac{\mathrm{i}G_3\mathrm{e}^{\mathrm{i}\boldsymbol{k}_3\cdot\boldsymbol{r}}}{D_2}\rho_{23}^{(3)}$ is obtained. In a similar way, $\rho_{23}^{(3)} = \dfrac{-\mathrm{i}G_3^*\mathrm{e}^{-\mathrm{i}\boldsymbol{k}_3\cdot\boldsymbol{r}}}{D_3}\rho_{20}^{(2)}$ is deduced. The solution of Eqs.(2), (3) and (4) is deduced as $\rho_{\mathrm{SWM}}^{(\mathrm{s1})} = \dfrac{-\mathrm{i}U_1\left|G_3\right|^2}{D_1^2D_2^2D_3}$, furthermore, the results of other ten chains (s2)–(s11) can be written as $\rho_{\mathrm{SWM}}^{(\mathrm{s2})} = \rho_{\mathrm{SWM}}^{(\mathrm{s3})} = \dfrac{\mathrm{i}U_1\left|G_3\right|^2}{D_1^3D_2D_4}$, $\rho_{\mathrm{SWM}}^{(\mathrm{s4})} = \dfrac{\mathrm{i}U_2\left|G_2\right|^2}{\Gamma_{00}D_5D_1^2D_2}$, $\rho_{\mathrm{SWM}}^{(\mathrm{s5})} = \dfrac{\mathrm{i}U_2|G_2|^2}{\Gamma_{00}D_6D_1^2D_2}$, $\rho_{\mathrm{SWM}}^{(\mathrm{s6})} = \dfrac{\mathrm{i}|G_2|^2U_2}{D_1^2D_4^2D_3}$, $\rho_{\mathrm{SWM}}^{(\mathrm{s7})} = \dfrac{\mathrm{i}|G_2|^2U_2}{D_1D_6D_4^2D_3}$, $\rho_{\mathrm{SWM}}^{(\mathrm{s8})} = \dfrac{\mathrm{i}|G_2|^2U_2}{D_1D_6D_2D_3D_4}$, $\rho_{\mathrm{SWM}}^{(\mathrm{s9})} = \rho_{\mathrm{SWM}}^{(\mathrm{s10})} = \dfrac{\mathrm{i}\left|G_2\right|^2G_2^*U_2}{D_1^2D_2D_3D_4}$ and $\rho_{\mathrm{SWM}}^{(\mathrm{s11})} = \dfrac{\mathrm{i}\left|G_2\right|^2U_2}{D_1D_2D_3D_4D_6}$, where $U_1 = G_1G_2(G_2')^*\exp[\mathrm{i}(\boldsymbol{k}_1 + \boldsymbol{k}_2 - \boldsymbol{k}_2')\cdot\boldsymbol{r}]$ and $U_2 = G_1G_3(G_3')^*\exp[\mathrm{i}(\boldsymbol{k}_1 + \boldsymbol{k}_3 - \boldsymbol{k}_3')\cdot\boldsymbol{r}]$.

The weak coupling field limit is considered, i.e. $\left|G_3\right|^2 \ll \Gamma_{20}\Gamma_{32}$ and $\left|G_3\right|^2 \ll \Gamma_{10}\Gamma_{13}$. Then, the solution is obtained from expression (6) as follows:

$$\rho_{\mathrm{DressedF1}}^{(3)} \approx 3\rho_{\mathrm{FWM}}^{(\mathrm{f1})} + \rho_{\mathrm{SWM}}^{(\mathrm{s1})} + 2\rho_{\mathrm{SWM}}^{(\mathrm{s2})}. \tag{9}$$

The first part in expression (9) corresponds to the two-photon resonant NDFWM (the perturbation chain is (f1)), while the remaining two terms correspond to a three-photon resonant six-wave mixing (the perturbation chains are (s1) and (s2)). Under the weak intensity condition: $\left|G_2\right|^2 \ll \Gamma_{13}\Gamma_{23}$ and $\left|G_2\right|^2 \ll \Gamma_{10}\Gamma_{20}$, there exists the following equation:

$$\rho_{\mathrm{DressedF2}}^{(3)} \approx \rho_{\mathrm{FWM}}^{(\mathrm{f2})} + \rho_{\mathrm{FWM}}^{(\mathrm{f3})} + 3\rho_{\mathrm{FWM}}^{(\mathrm{f4})} + 2\rho_{\mathrm{FWM}}^{(\mathrm{f5})} + 2\rho_{\mathrm{SWM}}^{(\mathrm{s2})} + \rho_{\mathrm{SWM}}^{(\mathrm{s4})} + \rho_{\mathrm{SWM}}^{(\mathrm{s5})} + \rho_{\mathrm{SWM}}^{(\mathrm{s6})} + \rho_{\mathrm{SWM}}^{(\mathrm{s7})} + \rho_{\mathrm{SWM}}^{(\mathrm{s8})}. \tag{10}$$

In expression (10), the first four terms correspond to the two-photon resonant NDFWM (the perturbation chains are (f2)–(f5)), while the remaining six terms correspond to the three-photon resonant six-wave mixing (the perturbation chains are (s2)–(s8)).

Since the four-wave mixing and six-wave mixing signals propagate along the same direction, they are indistinguishable from each other. Therefore the total signal is given by the coherent superposition of these two signals, i.e. $\rho_{10} = \rho_{10}^{(3)} + \rho_{10}^{(5)}$.

4. EIT and slow light phenomenon

4.1. V-type four-level system

Distinguished from the above calculation process, without any approximation used here, ten density matrix dynamic equations for the V-type four-level system in Fig.1 are written as

$$\frac{\partial \rho_{00}}{\partial t} = \gamma_{10}\rho_{11} + \gamma_{30}\rho_{33} + \mathrm{i}G_1^* \mathrm{e}^{-\mathrm{i}\boldsymbol{k}_1'\cdot\boldsymbol{r}}\rho_{10} - \mathrm{i}G_1 \mathrm{e}^{\mathrm{i}\boldsymbol{k}_1\cdot\boldsymbol{r}}\rho_{10}^* + \mathrm{i}G_3^* \mathrm{e}^{-\mathrm{i}\boldsymbol{k}_3'\cdot\boldsymbol{r}}\rho_{30} - \mathrm{i}G_3 \mathrm{e}^{\mathrm{i}\boldsymbol{k}_3\cdot\boldsymbol{r}}\rho_{30}^*, \tag{11}$$

$$\frac{\partial \rho_{11}}{\partial t} = \gamma_{21}\rho_{22} - \gamma_{10}\rho_{11} - \mathrm{i}G_1^* \mathrm{e}^{-\mathrm{i}\boldsymbol{k}_1'\cdot\boldsymbol{r}}\rho_{10} + \mathrm{i}G_1 \mathrm{e}^{\mathrm{i}\boldsymbol{k}_1\cdot\boldsymbol{r}}\rho_{10}^* + \mathrm{i}G_2^* \mathrm{e}^{-\mathrm{i}\boldsymbol{k}_2'\cdot\boldsymbol{r}}\rho_{21} - \mathrm{i}G_2 \mathrm{e}^{\mathrm{i}\boldsymbol{k}_2\cdot\boldsymbol{r}}\rho_{21}^*, \tag{12}$$

$$\frac{\partial \rho_{22}}{\partial t} = -\gamma_{21}\rho_{22} - \gamma_{23}\rho_{22} - \mathrm{i}G_2^* \mathrm{e}^{-\mathrm{i}\boldsymbol{k}_2'\cdot\boldsymbol{r}}\rho_{21} + \mathrm{i}G_2 \mathrm{e}^{\mathrm{i}\boldsymbol{k}_2\cdot\boldsymbol{r}}\rho_{21}^*, \tag{13}$$

$$\frac{\partial \rho_{33}}{\partial t} = -\gamma_{30}\rho_{33} + \gamma_{23}\rho_{22} + \mathrm{i}G_3 \mathrm{e}^{\mathrm{i}\boldsymbol{k}_3\cdot\boldsymbol{r}}\rho_{30}^* - \mathrm{i}G_3^* \mathrm{e}^{-\mathrm{i}\boldsymbol{k}_3'\cdot\boldsymbol{r}}\rho_{30}, \tag{14}$$

$$\frac{\partial \rho_{10}}{\partial t} = -D_1\rho_{10} + \mathrm{i}G_1\rho_{00} + \mathrm{i}G_2^* \mathrm{e}^{-\mathrm{i}\boldsymbol{k}_2'\cdot\boldsymbol{r}}\rho_{20} - \mathrm{i}G_1 \mathrm{e}^{\mathrm{i}\boldsymbol{k}_1\cdot r}\rho_{11} - \mathrm{i}G_3 \mathrm{e}^{\mathrm{i}\boldsymbol{k}_3\cdot\boldsymbol{r}}\rho_{13}, \tag{15}$$

$$\frac{\partial \rho_{20}}{\partial t} = -D_2\rho_{20} + \mathrm{i}G_2 \mathrm{e}^{\mathrm{i}\boldsymbol{k}_2\cdot\boldsymbol{r}}\rho_{10} - \mathrm{i}G_1 \mathrm{e}^{\mathrm{i}\boldsymbol{k}_1\cdot\boldsymbol{r}}\rho_{21} - \mathrm{i}G_3 \mathrm{e}^{\mathrm{i}\boldsymbol{k}_3\cdot\boldsymbol{r}}\rho_{23}, \tag{16}$$

$$\frac{\partial \rho_{13}}{\partial t} = -D_4\rho_{13} + \mathrm{i}G_2^* \mathrm{e}^{-\mathrm{i}\boldsymbol{k}_2'\cdot\boldsymbol{r}}\rho_{23} + \mathrm{i}G_1 \mathrm{e}^{\mathrm{i}\boldsymbol{k}_1\cdot\boldsymbol{r}}\rho_{03} - \mathrm{i}G_3^* \mathrm{e}^{-\mathrm{i}\boldsymbol{k}_3'\cdot\boldsymbol{r}}\rho_{10}, \tag{17}$$

$$\frac{\partial \rho_{23}}{\partial t} = -D_3\rho_{23} + \mathrm{i}G_2 \mathrm{e}^{\mathrm{i}\boldsymbol{k}_2\cdot\boldsymbol{r}}\rho_{13} - \mathrm{i}G_3^* \mathrm{e}^{-\mathrm{i}\boldsymbol{k}_3'\cdot\boldsymbol{r}}\rho_{20}, \tag{18}$$

$$\frac{\partial \rho_{30}}{\partial t} = -D_5\rho_{30} + \mathrm{i}G_3 \mathrm{e}^{\mathrm{i}\boldsymbol{k}_3\cdot\boldsymbol{r}}\rho_{00} - \mathrm{i}G_1 \mathrm{e}^{\mathrm{i}\boldsymbol{k}_1\cdot\boldsymbol{r}}\rho_{31} - \mathrm{i}G_3 \mathrm{e}^{\mathrm{i}\boldsymbol{k}_3\cdot\boldsymbol{r}}\rho_{33}, \tag{19}$$

$$\frac{\partial \rho_{21}}{\partial t} = -D_7\rho_{21} + \mathrm{i}G_2 \mathrm{e}^{\mathrm{i}\boldsymbol{k}_2\cdot\boldsymbol{r}}\rho_{11} - \mathrm{i}G_1^* \mathrm{e}^{-\mathrm{i}\boldsymbol{k}_1'\cdot\boldsymbol{r}}\rho_{20} - \mathrm{i}G_2 \mathrm{e}^{\mathrm{i}\boldsymbol{k}_2\cdot\boldsymbol{r}}\rho_{22}. \tag{20}$$

With the condition $\rho_{00}+\rho_{11}+\rho_{22}+\rho_{33} = 1$, the above equations are solved and the expression of ρ_{10} is obtained. Besides, the simulation results of absorption and population of diagonal density matrix elements are presented. In these equations, γ_{10}, γ_{21}, γ_{23} and γ_{30} are decay rates of levels $|0\rangle$-to-$|1\rangle$, $|1\rangle$-to-$|2\rangle$, $|2\rangle$-to-$|3\rangle$ and $|0\rangle$-to-$|3\rangle$, respectively.

According to the above equations, an accurate numerical simulation about EIT spectra, asymmetrical EIT and diagonal population during the whole process in a V-type four-level system can be carried out. An obvious EIT phenomenon is shown in Figs.4(a) and 4(b), in which the spectra of EIT absorption are plotted, with the laser intensity G_3 fixed but G_2 having three different values, and with G_2 fixed but G_3 having four different values, respectively, showing an explicit transparent EIT window in the absorption at probe detuning $\Delta_1 = 0$ when $\Delta_2 = \Delta_3 = 0$. As G_2 or G_3 changes the EIT spectra exhibit multiple peaks. There exist three effects: one-, two- and three-photon EIT effects, that can make contributions to these multiple peaks. As the SWM and FWM are probed in the same direction ρ_{10}, the phenomenon becomes complex. Therefore, this EIT phenomenon with multiple peaks is formed jointly by three effects, namely, one-, two- and three-photon EIT effects.

Figure 5(a) shows the asymmetrical EIT spectra under the condition $\Delta_2 = \Delta_3 \neq 0$, caused by a multiple photon interference effect. Figure 5(b) shows the population probability in ground state $|0\rangle$ and other excited states $|1\rangle$, $|2\rangle$ and $|3\rangle$ at laser intensities G_2 and G_3. The total population in the process of multiple-photon effect is a constant, which agrees well with the case under the condition $\rho_{00}+\rho_{11}+\rho_{22}+\rho_{33} = 1$. It is shown in Fig.5(b) that the two peaks and a central peak at $\Delta_1 = 0$ vary with laser intensity, so the multiple-photon effect also influences the spectra. These peaks are caused by one-photon resonance and

multiple-photon resonance, which are both enhanced by the constructive interference. Shown in Fig.5(c) are the squared values of dispersion and absorption, which separately make contributions to the signal intensity ($|\rho_{10}|^2$). From these spectra we can see that the signal intensity also has multiple peaks, which are caused by the one-, two- and three-photon resonances. The calculations show that the absorption makes more contributions to the total signal intensity than the dispersion.

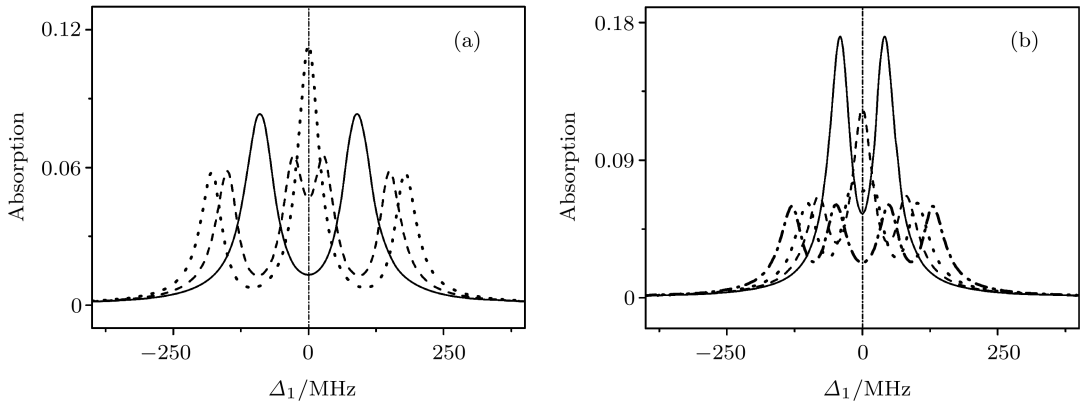


Fig.4. Numerical simulations of EIT spectra for the dispersion and absorption of a four-level system, (a) with G_3 fixed at 88.81 MHz, but G_2 taken as 5 (solid), 60 (dash), and 88.81 MHz (dash dot), and (b) with G_2 fixed at 39.72 MHz but G_3 taken as 10 (solid), 39.72 (dash), 60 (dot) and 88.81 MHz (dash dot). Parameters are taken as $\Delta_2 = \Delta_3 = 0$, $\gamma_{10} = 2\pi \times 5.4$ MHz, $\gamma_{21} = 2\pi \times 0.8$ MHz, $\gamma_{23} = 2\pi \times 0.97$ MHz, $\gamma_{30} = 2\pi \times 5.9$ MHz and $G_1/2\pi = 2$ MHz.

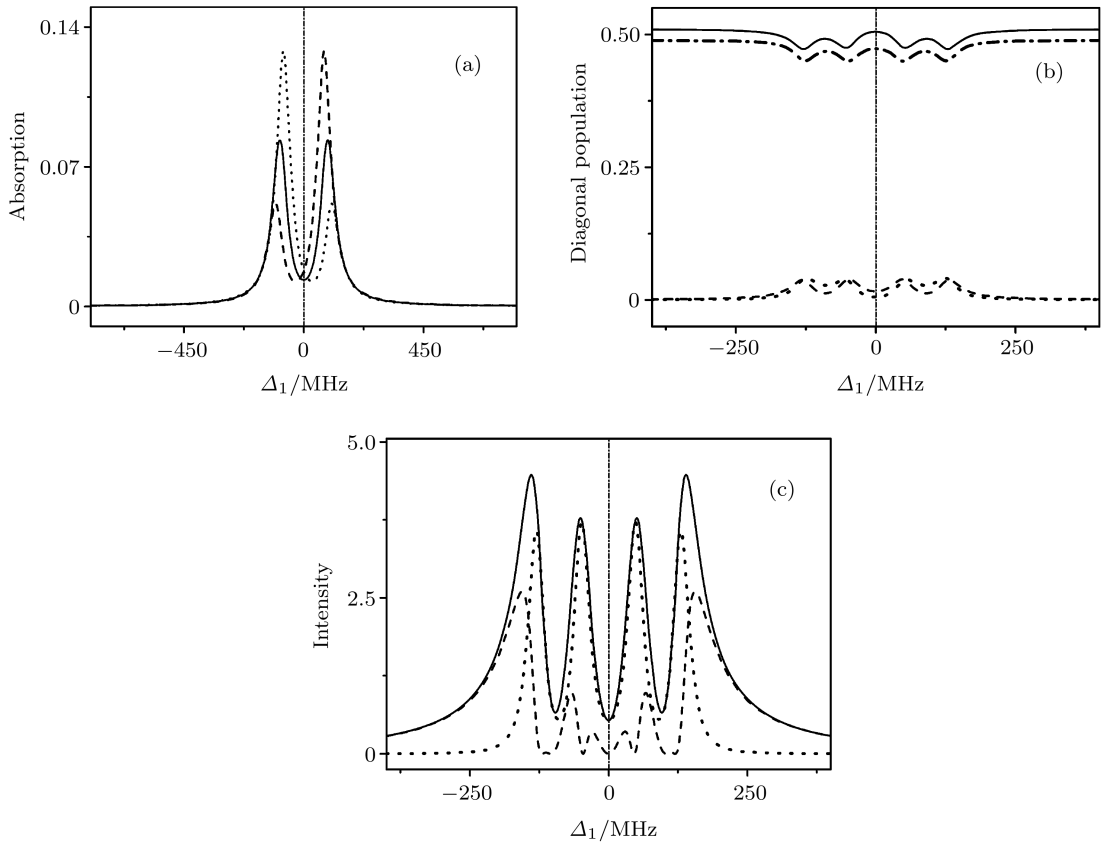


Fig.5. Asymmetrical EIT spectra for probe absorption scanning Δ_1 (a) with the parameters of $G_2 = 5$ MHz, $G_3 = 88.81$ MHz, $\Delta_2 = \Delta_3 = 0$ (solid), $\Delta_2 = -\Delta_3 = -30$ (dash), and $\Delta_2 = -\Delta_3 = 30$ (dot), three diagonal density matrix element populations ρ_{00} (solid), ρ_{11} (dash), and ρ_{22} (dot), (b) with the parameters of $\Delta_3 = \Delta_2 = 0$ and $G_3 = 88.81$ MHz and $G_2 = 39.72$ MHz, and (c) the signal intensity (solid), squared real part of ρ_{10} (dot) and squared imaginary part of ρ_{10} (dash). The intensities of spectra with parameters of $G_3 = 88.81$ MHz and $G_2 = 39.72$ MHz have been magnified 100 times.

4.2. Group speed and slow light phenomenon

The group speed of the probe (χ_1) is given by $v_{g1} = c/[1 + \omega_1(\partial\chi_1/\partial\omega_1)_{\Delta_1=0}/2]$. The multi-wave mixing group speed (see Fig.6)[4] is considered. Take the definition $K = N\mu_{10}/\varepsilon_0 E(\omega_1)$, then we will have $\chi(\omega_1) = K\rho_{10}$. Through the numerical calculation of Eqs.(11)–(20), a speed is acquired and the character of the slow light phenomenon is obtained. In the following the group speed in this V-type four-level system is discussed.

Figure 6 shows a multi-wave mixing group speed versus laser intensities G_2 (Fig.6(a)) and G_3 (Fig.6(b)). Both Fig.6(a) and Fig.6(b) show a phenomenon with several points where the group speed reaches a minimum. In Fig.6(a), when the value of G_2 is relatively small in a arrange from 0 to 100 MHz, there exists a minimal point of V_g where $V_g < c$, and as G_2 increases, the group speed takes on a feature of superluminal light propagation. While the value of G_2 enters into a range from 100 to 300 MHz as it increases continually, the group speed shows a superluminal phenomenon again and at the G_2 value near 114MHz, the group speed reaches a slow light point $V_g < c$. And in Fig.6(b), there exist two points of minimal group speed of light ($V_g < c$) when G_3 increases with G_2 value, which is similar to what is exhibited in Fig.6(a).

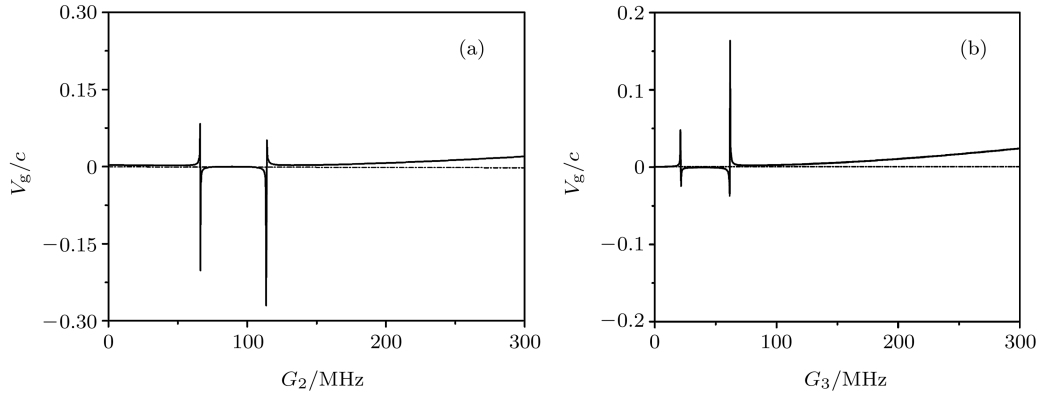


Fig.6. Group speed of multi-wave mixing versus G_2 with the parameters of $G_3 = 88.81$ MHz and $K \approx 0.035$ (a), and versus G_3 with the parameter of $G_2 = 39.72$ MHz (b).

5. Discussion and conclusion

In this paper, by blocking the laser $\boldsymbol{k}_3'$ or $\boldsymbol{k}_2'$, two-photon resonant NDFWM in a dressed V-type four-level system has been investigated, with a coupling field under two different dressed FWM conditions. Two- and three-photon AT splitting phenomena under these two conditions are simulated, the results show obvious intensity splitting with the enhancement and suppression spectra present.

Meanwhile, the EIT phenomena are obtained in the V-type four-level system. In this system, the EIT phenomena show multiple peaks as the pump or coupling field intensity increases. There are three effects that can make contributions to the whole process, namely, one-, two- and three-photon resonances. With the investigation of EIT phenomena, a multi-wave mixing group speed propagating through the EIT medium is obtained, and at a certain pump or coupling field intensity, its speed is slower than the speed of light in vacuum. Furthermore, when pump or coupling field increases, the slow light propagation presents multiple minimum points at a certain value of laser intensity.

References

[1] Harris S E 1997 *Phys. Today* **50**(7) 36
[2] Xiao M, Li Y Q, Jin S and Gea-Banacloche J 1995 *Phys. Rev. Lett.* **74** 666
[3] Kang H and Zhu Y F 2003 *Phys. Rev. Lett.* **91** 093601
Wu Y 2005 *Phys. Rev.* A **71** 053820
[4] Zhang Y P, Brown A W and Xiao M 2006 *Phys. Rev.* A **74** 053813
[5] Zhang Y P, Gan C L and Xiao M 2006 *Phys. Rev.* A **73** 053801
[6] Sun J, Zuo Z C, Mi X, Yu Z H, Wu L A and Fu P M 2005 *Acta Phys. Sin.* **54** 149 (in Chinese)